Supporting Information

Direct structural evidence for interfacial gradients in asymmetric polymer nanocomposite blends

Anne-Caroline Genix,[1*] Vera Bocharova,[2] Bobby Carroll,[2] Philippe Dieudonné-George,[1] Michael Sztucki,[3] Ralf Schweins,[4] Alexei P. Sokolov,[2,5] and Julian Oberdisse[1]

[1]*Laboratoire Charles Coulomb (L2C), Université de Montpellier, CNRS, F-34095 Montpellier, France*

[2]*Chemical Sciences Division, Oak Ridge National Laboratory, Oak Ridge, TN 37831, USA*

[3]*European Synchrotron Radiation Facility, 71 Avenue des Martyrs, CS 40220, F-38043 Grenoble Cedex 9, France*

[4]*Institut Laue-Langevin, DS/LSS, 71 Avenue des Martyrs, CS 20156, F-38042 Grenoble Cedex 9, France*

[5]*Department of Chemistry, University of Tennessee, Knoxville, TN 37996, USA*

* Corresponding author: anne-caroline.genix@umontpellier.fr

I. Silica-free H/D blends

The scattered intensities of several H/D blends measured by SANS are shown in Figure S1. Data at intermediate and high-q are well-described by the random phase approximation proving molecular mixing of the H- and D-chains of different masses. The low-q upturn is found to be independent of molecular weight.

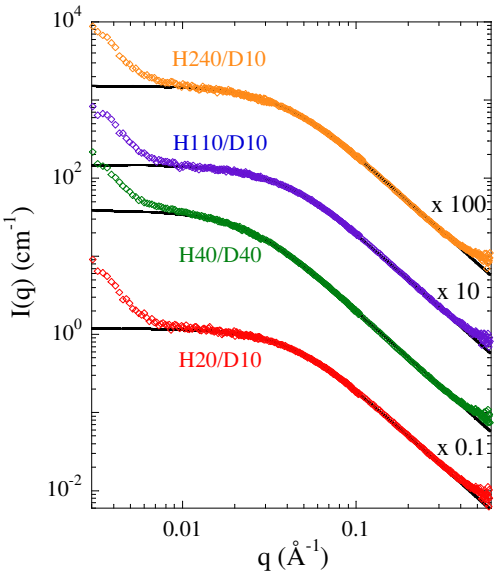

Figure S1. Scattered SANS intensity of pure symmetric H40/D40 and three asymmetric PVAc blends (H20/D10, H110/D10 and H240/D10, vertically shifted x1/10, x10 and x100, respectively), compared to the RPA fit with χ = 0 corresponding to the average of the Debye form factors with parameters given in Table 1.

II. Characterization of silica nanoparticles

Two colloidal suspensions with silica nanoparticles (NPs) of different size were characterized by SAXS after dilution in ethanol. The scattered intensities were fitted with log-normal distributions of spherical objects in Figure S2 demonstrating a good NP dispersion in ethanol. The characteristic sizes are summarized in Table S1.

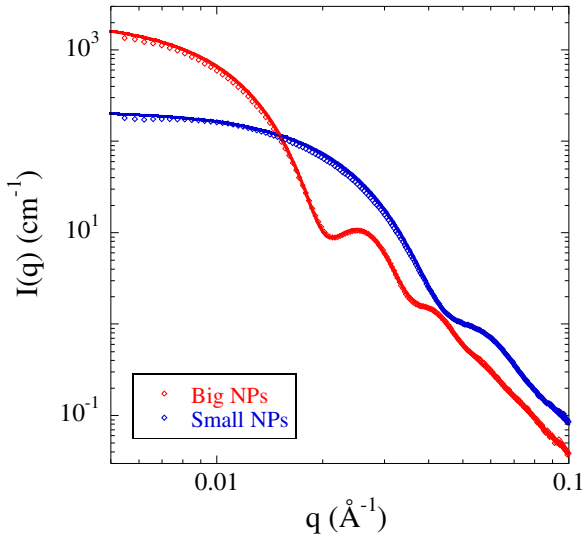

Figure S2. SAXS intensities (symbols) and modeling by log-normal distributions (lines) of spherical particles of colloidal silica suspensions diluted in ethanol (Φ_{NP} = 0.3%v).

Table S1. Summary of particle sizes. σ is the polydispersity, <R> is the average radius and ρ_{NP} is the scattering length density of silica NPs.

Sample	R_0 (nm)	σ (%)	<R> (nm)	ρ_{NP} (10^{10} cm^{-2})	density ($g.cm^{-3}$)
Small silica NPs	9.37	17.0	9.51	3.59	2.271
Big silica NPs	21.18	12.2	21.33	3.63	2.296

III. Contrast variation experiments

We used the contrast-variation method to determine the scattering length densities of the big silica NPs and the deuterated PVAc with MW = 39.6 kg/mol (D40). Contrast variations of the small silica NPs, protonated PVAc (MW = 15 kg/mol) and deuterated PVAc with MW = 13 kg/mol are reported in the supplementary information of [1]. The batch of big silica NPs (Table S1) has been studied after dialysis in ethanol in order to remove water residues. Four dilutions in mixtures of protonated/fully deuterated ethanol have been used for the big silica NPs (Φ_{NP} = 0.35%v), whereas acetone mixtures were used for D40 PVAc (Φ_{pol} = 2%v). Figures S3 displays the contrast variation results measured by SANS. The resulting scattering length density of silica, ρ_{NP}, is given in Table S1 with the corresponding density. The scattering length density of D40 PVAc is 7.02 10^{10} cm^{-2}, i.e., the same as for D-PVAc with MW = 13 kg/mol.

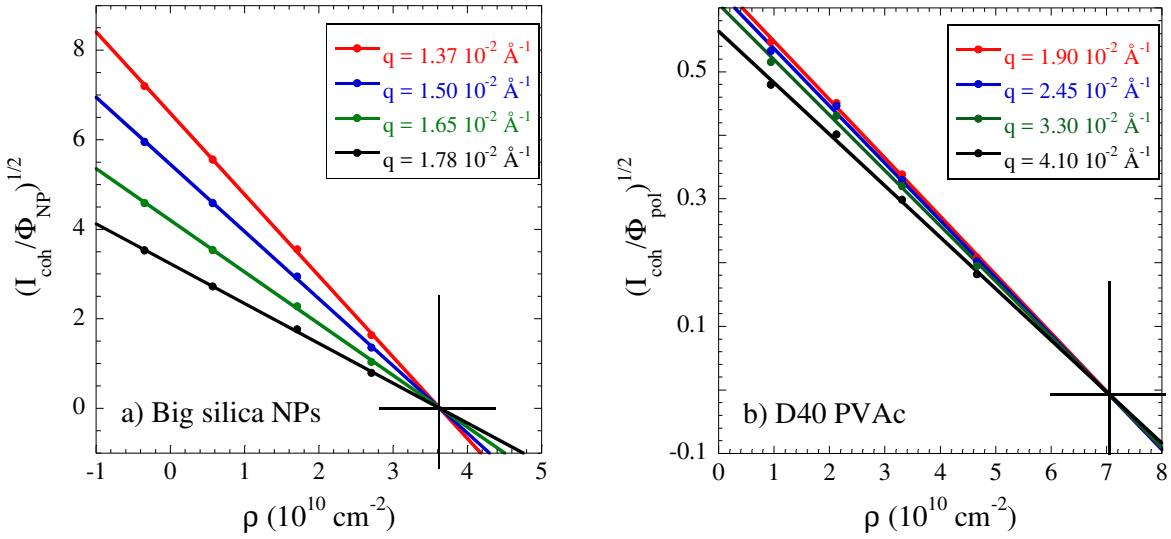

Figure S3. Contrast variations by SANS for big silica NPs diluted in ethanol (**a**), and deuterated PVAc (D40, MW = 39.6 kg/mol) in acetone (b). ρ is the solvent scattering length density.

In order to fulfill the zero-average contrast condition, [2] ρ_{NP} has to match the average of the polymer mixture $\rho_{H/D} = \Gamma_H \rho_H + \Gamma_D \rho_D$. The matching point of the big silica NPs is found at a matrix volume fraction in hydrogenated polymer $\Gamma_H = 60\%$ ($\Gamma_H + \Gamma_D = 100\%$). For small NPs, matching is obtained at $\Gamma_H = 61\%$ (see SI in [1]).

IV. Filler structure in PNC blends

The SAXS results for the PNC blends shown in Figure 2 (SANS data) are presented in Figure S4.

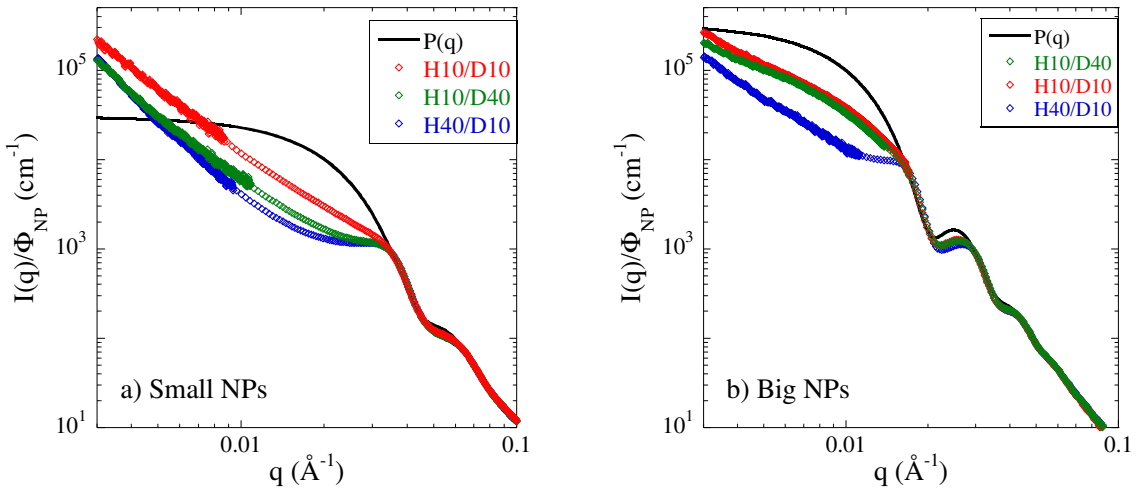

Figure S4. Normalized scattered SAXS intensity of PNCs with symmetric H10/D10 ($\alpha \approx 1$) and two asymmetric blends (H10/D40, $\alpha = 0.26$; H40/D10, $\alpha = 4.1$), for **(a)** small silica NPs, and **(b)** big silica NPs. The volume fraction of silica is ca. 8%v. The corresponding particle form factors are shown for comparison (black lines).

One may note that in both figures the form factor oscillation is not perfectly reproduced by the theoretical function, although this is perfectly the case in Figure S2. This is caused by the considerable difference in concentration, which makes the structure factor not only modify the low-q scattering with the correlation hole and the low-q increase, but also shifts the oscillations, as pointed out in [1].

V. Form factor of a fuzzy sphere

The scattering of fuzzy spheres has been described in various ways in the literature. [3-5] The easiest expression is the product of the normalized hard sphere form factor $P_{sphere}(q, R)$ by a Gaussian:

$$V_{fuzzy}^2 P_{fuzzy}(q, R, \sigma) = (A V_{sphere})^2 \; P_{sphere}(q, R) \; \exp(-q^2\sigma^2) \qquad (S1)$$

where A is a constant to be determined below, and V_{fuzzy} the volume of the fuzzy sphere. The theoretical justification of this expression is that the product in q-space corresponds to a convolution in r-space, by the Gaussian $\exp(-(r-r')^2/2\sigma^2)$ which has to be normed to one taking into account the cut-off at r = 0. It is, however, not clear in the literature if the corresponding volume term is adjusted from its perfect sphere value $V_{sphere} = 4\pi/3\ R^3$, with possible (but minor, see below) consequences on the use of absolute intensity values, and thus particle masses for example. We have therefore recalculated the volume term by numerical integration. An example of the radial density is shown in Figure S5, for convolutions with different σ given as fraction of the radius σ/R, here R = 10 nm.

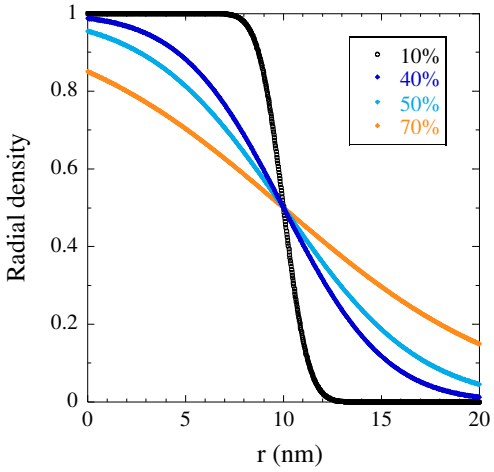

Figure S5. Radial density profiles for a fuzzy particle of radius R = 10 nm and different fuzziness σ.

Obviously, for large σ, the upper bound of the integration must be adjusted to higher r than shown in the plot, but the lower bound is always zero. Consequently, the correct normalization constant of the convolution must be recalculated in all cases. Next, the integral over the profile describing the density function contains a volume term $4\pi\ r^2$, which is thus asymmetric around r = R, and increases the weighting of the outer zones of higher r. To fix ideas, in the case of a 10% interfacial width (σ/R = 10%), the correction factor is A = 1.03, and for 20%, it is A = 1.12.

Finally, it is thus possible to calculate numerically the P_{fuzzy}-term by numerical integration of the smooth density profile, and compare it to the one given by eq. (S1), and to the hard sphere form factor. To facilitate this optically, we have renormed all three to one at low angles, but both fuzzy terms still need to be multiplied by the prefactor A before being used quantitatively. The effect of fuzziness is to increase the particle size visible in the Guinier regime, as well as the enveloping high-q power law to a value

steeper than the Porod law, thereby decreasing the higher-order form factor oscillations, as expected for fuzziness.

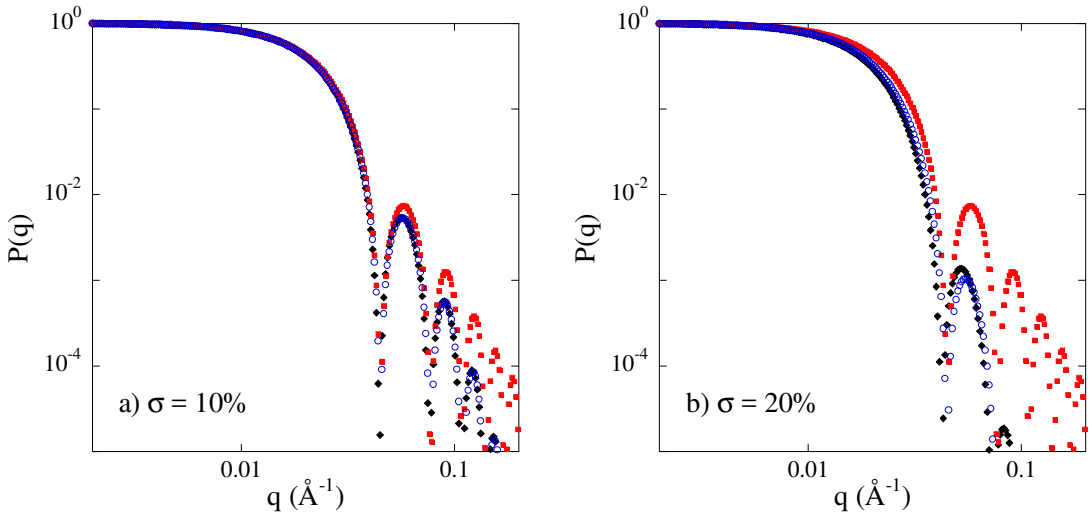

Figure S6. Comparison of hard spheres form factor (red symbols), and fuzzy sphere calculated using eq. (S1) (blue symbols), or the numerical integration (black symbols), for **(a)** σ = 1 nm, and **(b)** σ = 2 nm, for a nominal radius of 10 nm.

VI. Characteristics of the segregated zones

VI. 1. Impact of the number density

As a representative example, the SANS scattering data of PNC H10/D40 with small NPs have been fitted using eq. (6) and varying the number density of segregated zones, N_{seg}. Several choices of the ratio N_{seg}/N_{NP} where N_{NP} is the number density of silica particles have been considered in Figure S7a. The scattered intensity is equivalently well-described for N_{seg}/N_{NP} values between 0.25 and 1.5. In this range, the radius of segregated zones is constant (ca. 15.8 nm) and only the "visibility" of segregation $\Delta\Gamma_H^{seg}$ is found to decrease to compensate the corresponding increase in Φ_{seg}. This allows maintaining constant the SANS prefactor as the contribution of the segregated zones dominates at low-q. The evolution of the prefactor of the segregated zones, $\Delta\rho_{seg}^2\ \Phi_{seg}\ V_{seg}$, is plotted in Figure S7b together with the segregation parameter Θ_{seg} (eq. (9)). The latter is found to decrease with increasing the number of fuzzy ball per silica NP.

Using N_{seg}/N_{NP} values out of the range [0.25 – 1.5] leads to non-satisfactory fits as illustrated in Figure S7a, and to different R_{seg} in order to adjust the SANS prefactor: R_{seg} = 19 nm (upper limit of R_{seg}) and 13.8 nm for N_{seg}/N_{NP} = 0.1 and 1.75, respectively. A natural choice was thus to fix N_{seg}/N_{NP} to 1, which is illustrated by the point in the middle in Figure S7b. The arrows indicate possible variations to smaller or larger values, which however remain within a rather small range centered around the silica particle density, without impacting the other fit parameters.

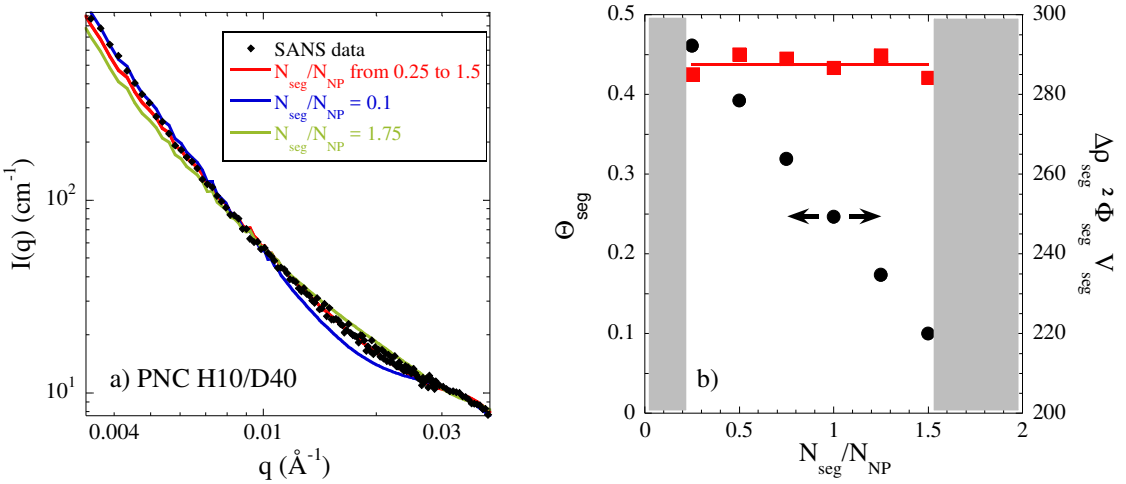

Figure S7. (a) Scattered SANS intensity of PNC H10/D40 with small silica NPs (α = 0.26; Φ_{NP} = 9.2%v). Lines are fits to the SANS data following eq. (6) and considering different values of N_{seg}/N_{NP} as indicated in the legend. **(b)** Average degree of H/D segregation (black circles) and SANS prefactor of the segregated zones (red squares) as a function of N_{seg}/N_{NP}.

VI. 2. Structure factor

Two options for the structure factor of the segregated zones have been considered in Figure S8. The first one, called "uncorrelated", assumes a random distribution in space (S_{seg} = 1 in eq. (6)). It is seen to highlight the form factor of these zones, which eventually gain intensity around the low-q upturn, which is related to their radius. This approach, however, fails in describing the entire intensity. If one chooses to confer a spatial organization to segregated zones identical to the one of silica NPs ($S_{seg} = S_{NP}$ with S_{NP} deduced from the SAXS measurement), then the low-q upturn can be captured rather well ("correlated" in Figure S8).

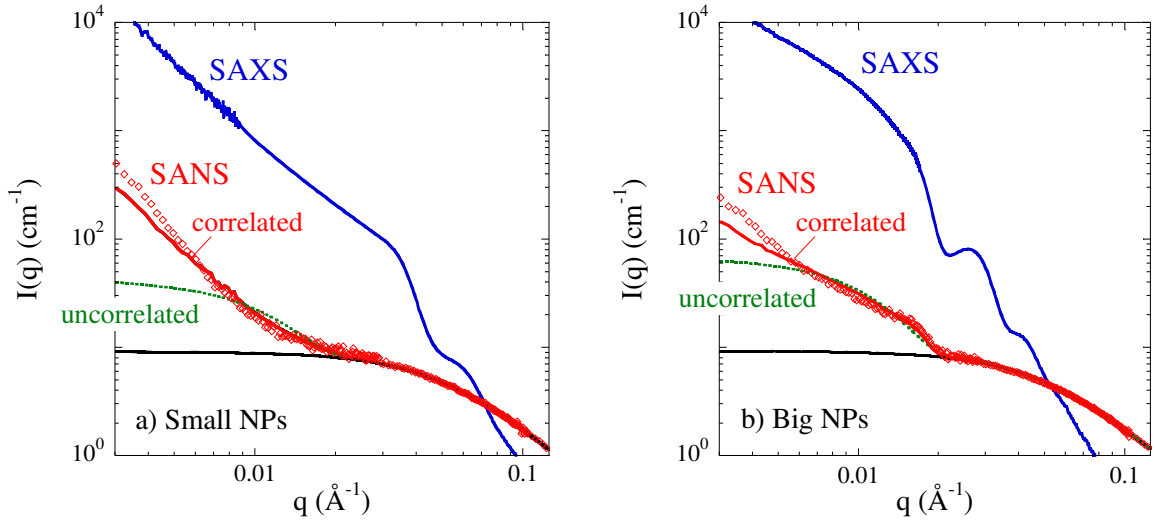

Figure S8. Scattered SANS intensity of symmetric H10/D10 nanocomposites ($\alpha \approx 1$), compared to the silica structure measured by SAXS of the same samples. Chain scattering is described by RPA using the Debye form factor as described in the text (black line). The effect of correlating the segregated zones using the silica structure factor is illustrated by their respective fits. **(a)** Small silica NPs (Φ_{NP} = 6.9 %v), **(b)** big silica NPs (Φ_{NP} = 6.4 %v).

VI. 3. Evolution of the radius R_{seg}

The size of the segregated zones is a free fit parameter of our model, while the fuzziness has been fixed to 20% as motivated below. In Figure S9, we have plotted the resulting R_{seg} as a function of matrix asymmetry, for small and big silica beads. The size of the zones is smaller for the smaller silica beads, approximately in accordance with the decrease in radius, and their evolution follows an identical power law. The remarkable feature is that there seems to be no discontinuity at $\alpha = 1$, although interfacial segregation leading to the scattering peak sets in at this point. We interpret this as a sign of independence of bulk segregation (which always happens, evolving continuously with the matrix composition) from interfacial segregation.

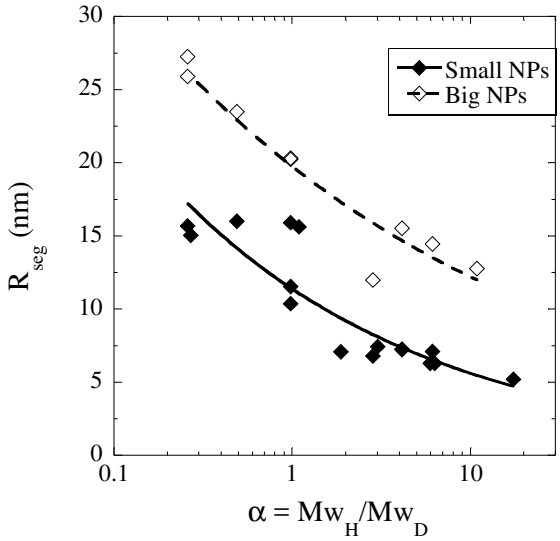

Figure S9. Radius of segregated zones as a function of matrix asymmetry parameter. Full and empty symbols are for PNCs filled with small and big NPs, respectively. Data are described by a power law with a negative exponent of ca. 0.2 - 0.3.

VII. SANS spectra for PNC blends

VII. 1. $\alpha \leq 1$

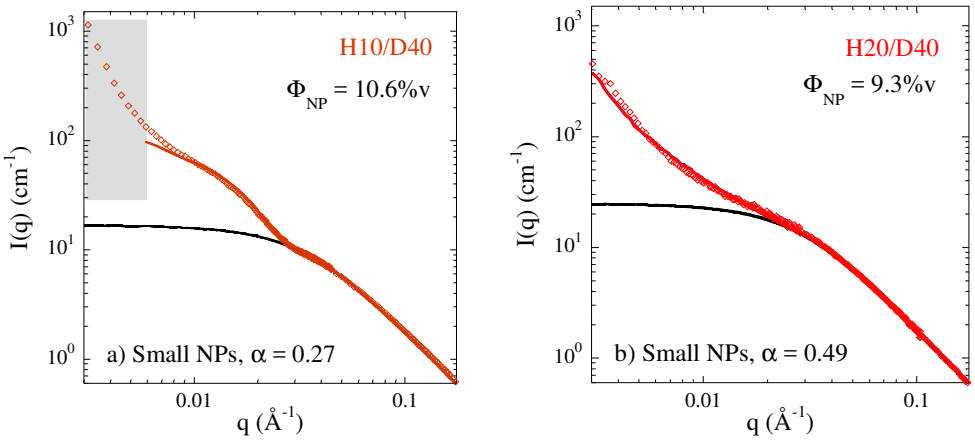

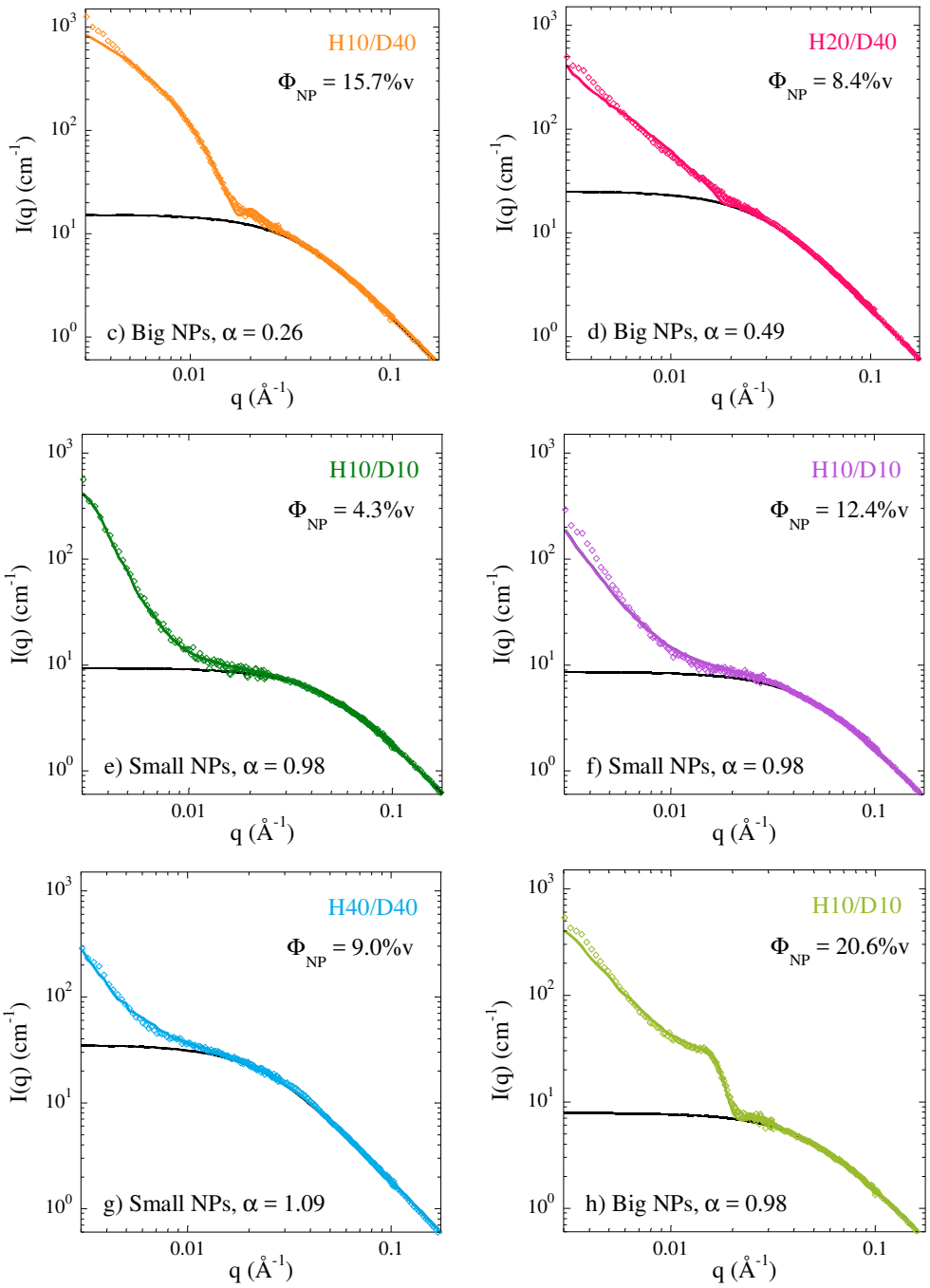

Figure S10. Scattered SANS intensity of H/D PNC blends with different asymmetry parameters. $\alpha < 1$ in **(a)-(b)** with small NPs and **(c)-(d)** with big NPS, and $\alpha \approx 1$ in **(e)-(f)-(g)** with small NPs and **(h)** with big NPs. Chain scattering is described by RPA using the Debye form factor as described in the text (black line). The best fit using correlated segregated zones described by fuzzy balls (eq. (6)) is shown as solid line through the experimental points. For PNC H10/D40 in **(a)**, the low-q SAXS data were not measured and fit of the SANS intensity has been performed over a limited q-range as highlighted by the grey square.

VII. 2. α > 1 and small silica NPs

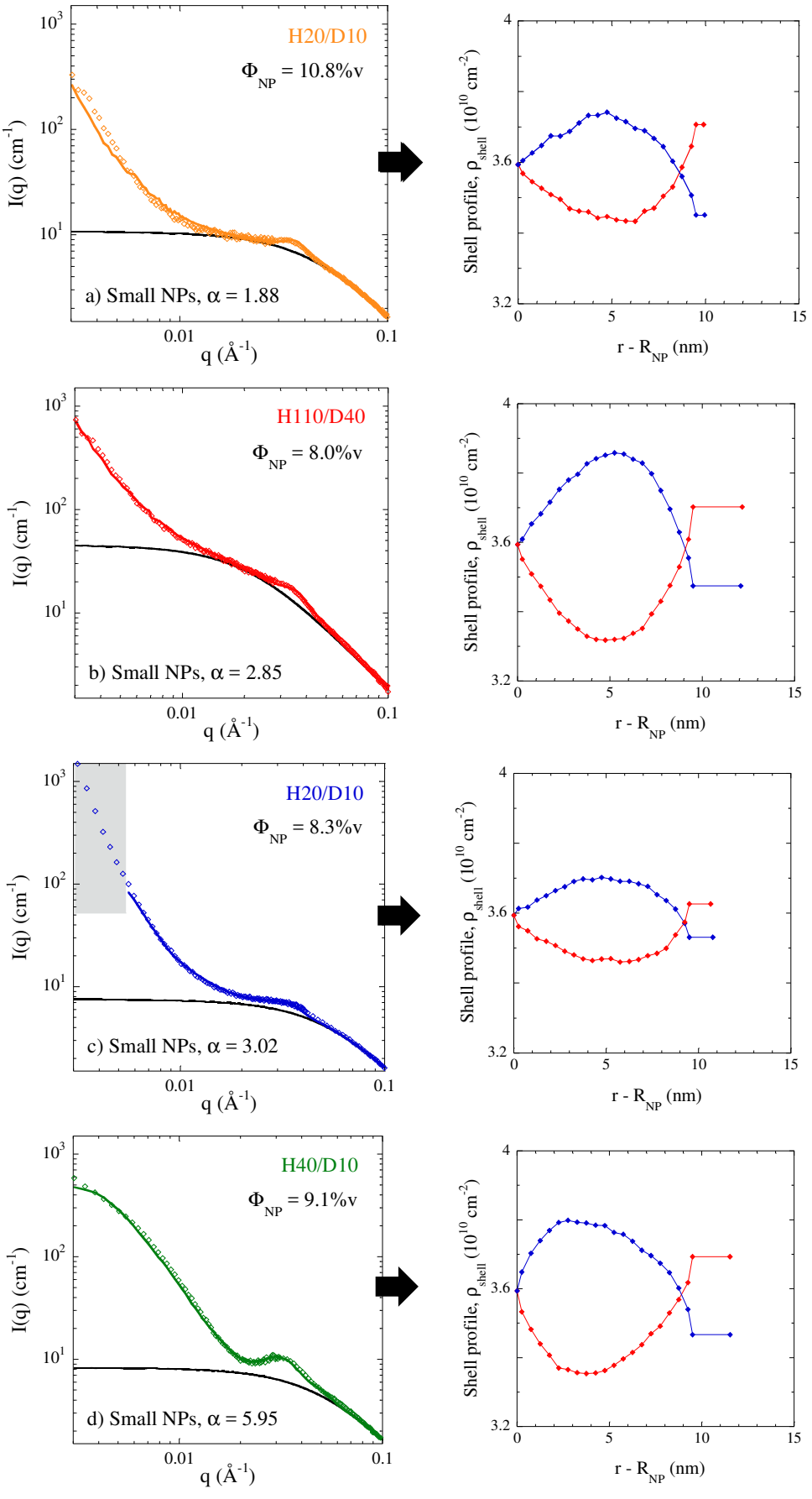

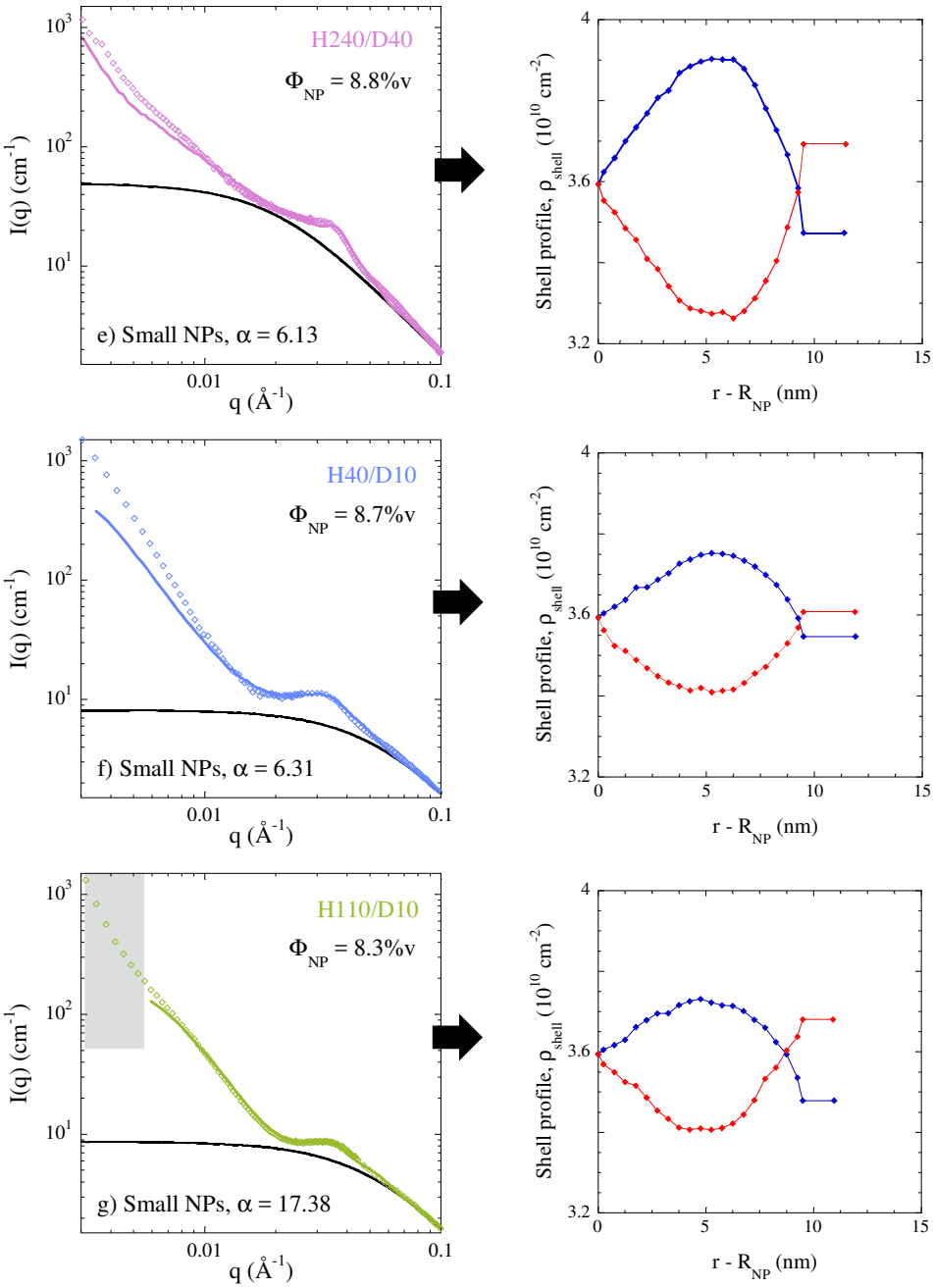

Figure S11. Scattered SANS intensity of H/D PNC blends with asymmetry parameter $\alpha > 1$ and small silica NPs ($R_{NP} \approx 10$ nm) **(a)**, **(b)**, **(c)**, **(d)**, **(e)**, **(f)** and **(g)**. Chain scattering is described by RPA using the Debye form factor as described in the text (black line). The best fit using correlated segregated zones and an isotopically visible shell (eqs. (7) and (8)) is shown as solid line through the experimental points. In **(c)** and **(g)**, the low-q SAXS data were not measured and fit of the SANS intensity has been performed over a limited q-range as highlighted by the grey square. Fish-like scattering length density profiles within the shell are shown on the right.

VII. 3. α > 1 and big silica NPs

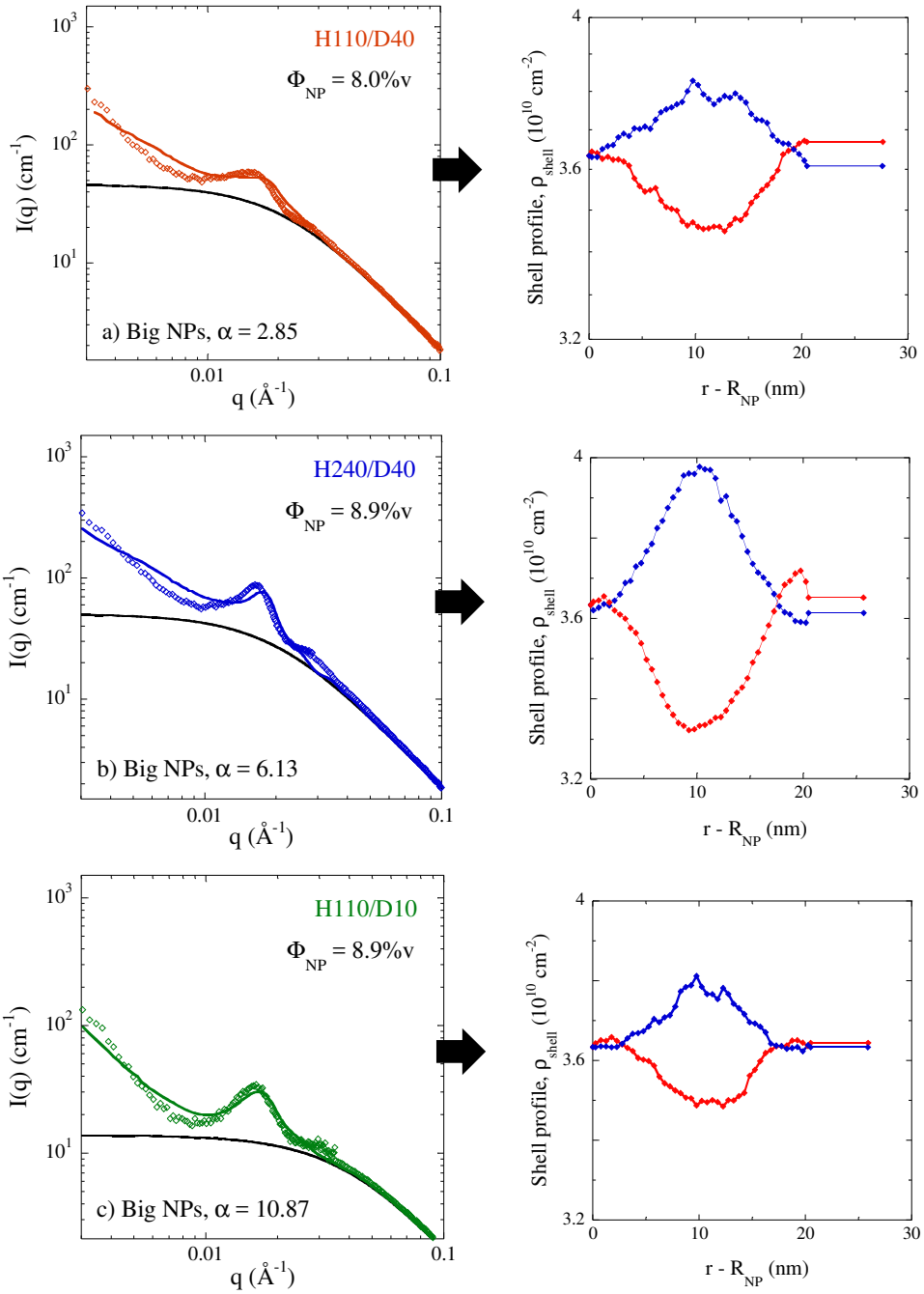

Figure S12. Scattered SANS intensity of H/D PNC blends with asymmetry parameter α > 1 and big silica NPs (R_{NP} ≈ 20 nm) **(a)**, **(b)** and **(c)**. Chain scattering is described by RPA using the Debye form factor as described in the text (black line). The best fit using correlated segregated zones and an isotopically visible shell (eqs. (7) and (8)) is shown as solid line through the experimental points. Fish-like scattering length density profiles within the shell are shown on the right.

VIII. Impact of fuzziness

The fuzziness parameter σ has been fixed to 20% in the description of the segregated zones in eqs. (6) and (7). Varying σ from 0 up to 40% was found to have no influence on the fit quality (Figure S13a). It also did not alter the fish-like shape of the shell profile as illustrated in Figure S13b. Starting from 50%,

slightly worst fits are obtained and the fish-like profiles are deformed. This is due to the contribution of the form factor of the segregated zones to the intensity peak. A too fuzzy interface results in a shift of the Guinier zone to lower q, weakening the amplitude of the predicted peak considerably below the measured intensity. As a result, fixing the fuzziness to 20% appears to be a reasonable choice which is consistent with the physical picture and with the possible parameter range.

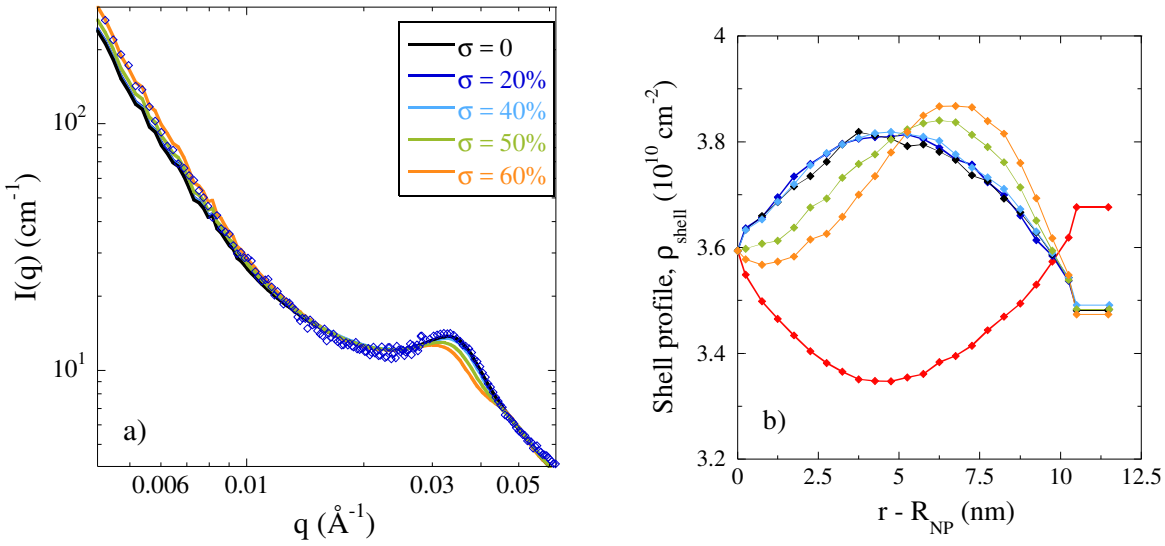

Figure S13. (a) Scattered SANS intensity of H40/D10 PNC with small silica NPs (α = 4.13; Φ_{NP} = 8.7%v). Lines are fits to the SANS data following eq. (7) and considering different values of fuzziness as indicated in the legend. **(b)** Corresponding scattering length density profiles within the shell.

IX. Additional results for big silica NPs

IX.1. Normalized polymer fractions

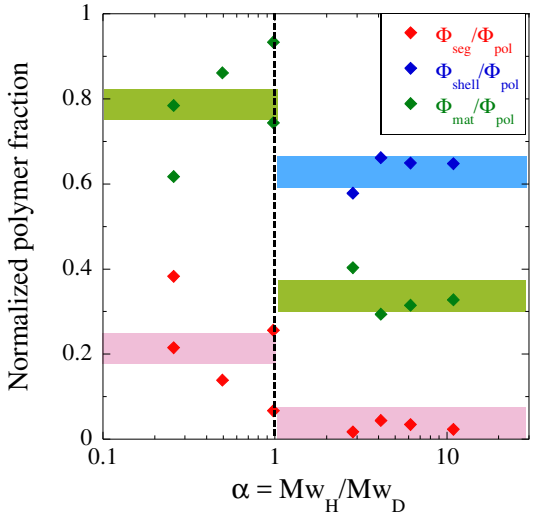

Figure S14. Normalized polymer fractions Φ_{shell}/Φ_{pol}, Φ_{mat}/Φ_{pol}, and Φ_{seg}/Φ_{pol} as a function of matrix asymmetry parameter for PNCs filled with big NPs. Colored bars are guides to the eye for the average polymer fractions and their dispersion.

IX.2. Decomposition

Fits of the SANS data of H10/D40 and H40/D10 PNCs filled with big silica NPs are decomposed in Figure S15. The fit of H10/D40 PNC is decomposed into the different contributions of eq. (6) – segregated zones, chain scattering and NP contribution due to the slight deviation of the ZAC condition – in Figure S15a. The slight hump located at ca. 7.10^{-3} Å^{-1} is created by the model geometry chosen for the segregated zones (fuzzy spheres of radius R_{seg} = 27.2 nm causing a Guinier-like scattering function, i.e., a characteristic low-q decrease). The hump can be seen to come from the superposition of the fuzzy form factor with the silica structure.

The fit of H40/D10 PNC is decomposed into the different contributions of eq. (7) in Figure S15b, and compared to the silica structure measured by SAXS of the same sample.

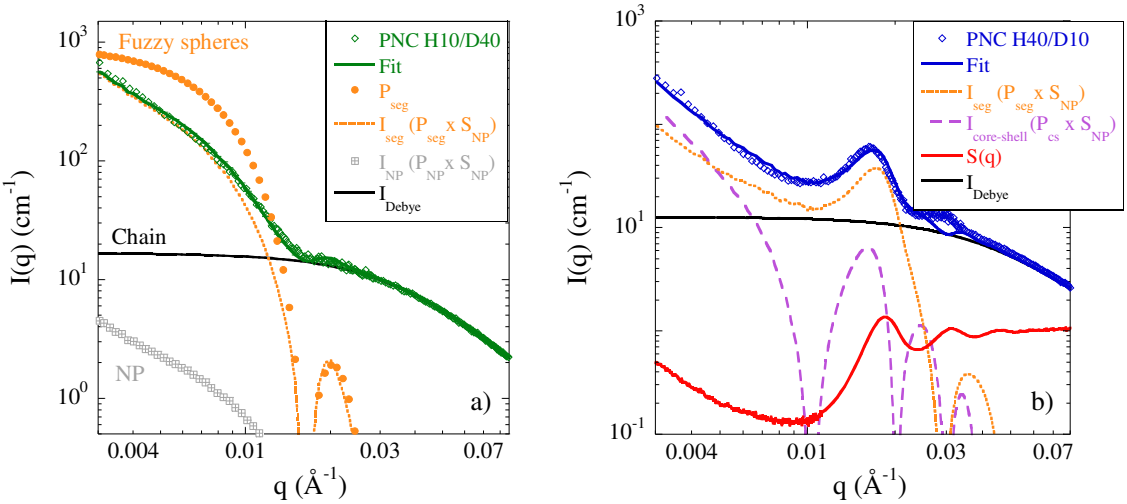

Figure S15. Scattered SANS intensities of asymmetric H10/D40 PNC (α = 0.26, Φ_{NP} = 8.3 %v) **(a)** and H40/D10 PNC (α = 4.1, Φ_{NP} = 9.1 %v) **(b)** filled with big silica NPs. Green and blue lines are fits to the SANS data. The different contributions are indicated in the caption. In **(b)**, data are compared to the silica scattering measured in independent SAXS experiment (S(q), red curve). The purple dashed line and the orange dotted line correspond to the contributions of the contrasted polymer shell and the segregated zones, respectively. Chain scattering (black line) is described by RPA using the Debye form factor as described in the text.

X. Fit with a single type of segregation for α > 1

Both interfacial and bulk segregations are required to describe the SANS data of PNCs with α > 1. Using only one type of segregation does not allow reproducing the experimental data as shown in Figure S16.

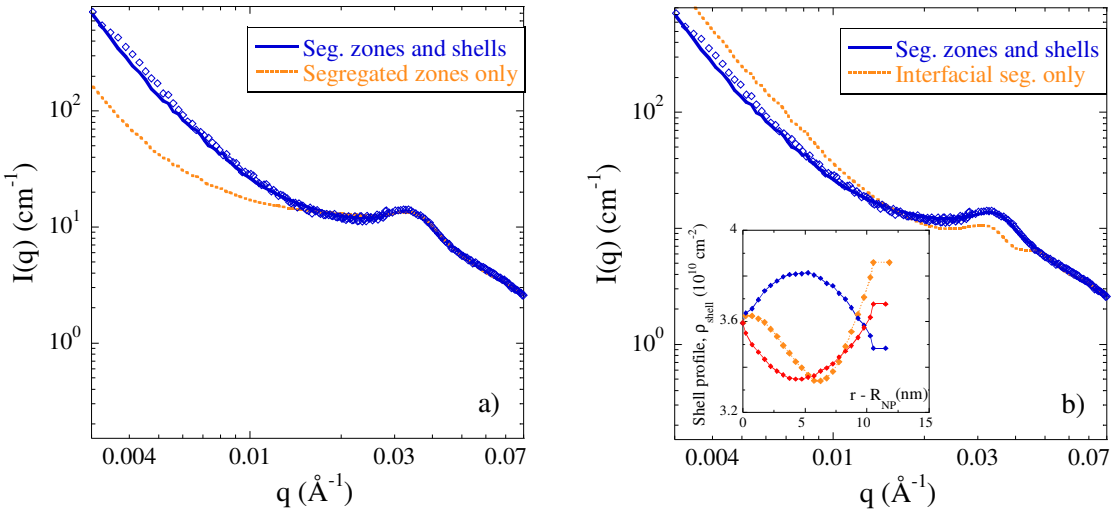

Figure S16. Scattered SANS intensity of PNC H40/D40 with small silica NPs (α = 4.13; Φ_{NP} = 8.7%v). Line is the best fit using eq. (7), i.e. adding both types of segregation. Dotted lines are fits to the experimental data considering only segregated zones with σ = 20% in **(a)** and only contrasted polymer shells in **(b)**. In (b), the corresponding shell profile is included in inset.

XI. Modeling of interfacial segregation

We estimate that a rather low number of zones effectively interferes with the silica-polymer shell, as only first neighbors may be present due to the crowding and the identical number densities of silica and segregated zones. It is sufficient to perform the calculation for one segregated zone, and possibly multiply by the number of neighbors, N'_{seg}, which we use as a free parameter. The distance distribution is more difficult to evaluate, as here the silica-segregation cross-correlation function would be needed, which is unfortunately inaccessible. We thus introduce Δ as the free parameter describing the average surface-to-surface distance between the silica particle and the segregated zones – taking R_{seg} to identify the position of its fuzzy surface. Δ is set to zero when the two touch, and it is negative when some "penetration" of the segregated zones into the silica NP is described. The silica being impenetrable, this situation corresponds to segregated zones squeezed onto the silica. The corresponding polymer is then redistributed to maintain volume conservation.

In Figure S17, the fuzzy segregated polymer zone located next to a silica particle is represented by dots of number density proportional to the number of monomers per unit volume. The fuzziness is described by a radial density profile (σ = 20%). The impact of this fuzzy zone on the scattering of the silica (with its polymer shell) can be quantified by the number of monomers in a spherical shell around the silica.

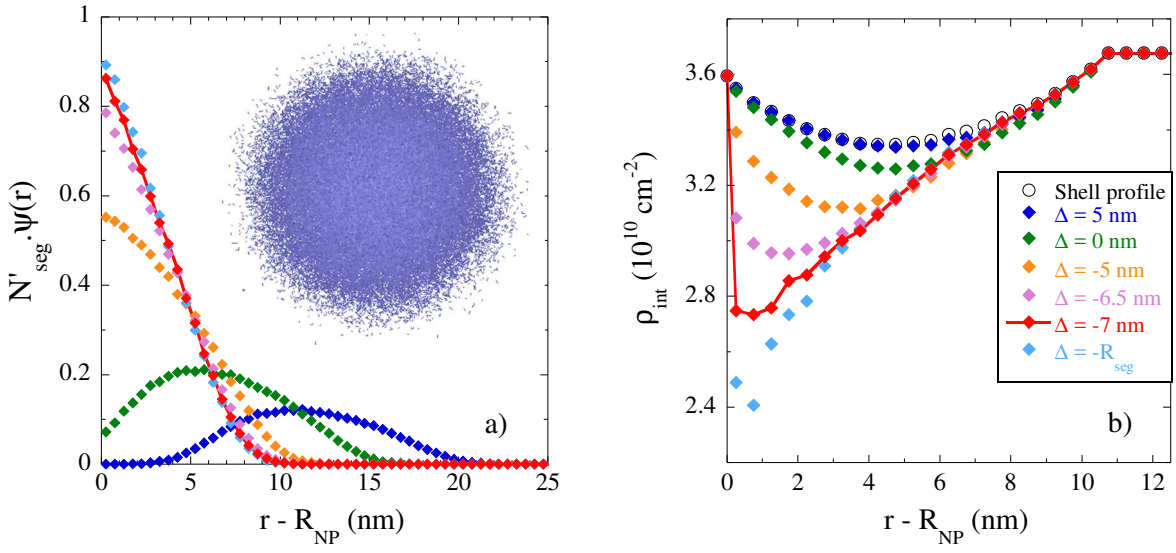

Figure S17. **(a)** Volume fractions of the shell occupied by the fuzzy sphere for different Δ values as indicated in the caption and N'_{seg} = 4. **(b)** The corresponding gradient profiles at the NP surface calculated using eq. (11) for H40/D10 PNC with small NPs (α = 4.1, Φ_{NP} = 8.7 %v). Red diamonds with the solid line represent the most plausible evolution of the interfacial profile with an enrichment in H chains. The inset illustrates a fuzzy sphere with σ = 20%, R_{seg} = 7.2 nm.

In Figure 7c, the volume fraction of the shell occupied by the fuzzy sphere is called ψ(r). Obviously, it depends on the radius of the shell, as well as on the distance between the silica and the segregated zone Δ. ψ(r) also allows us to take the squeezing effect into account for negative Δ, as the function is simply multiplied by a constant in order to maintain the total fuzzy volume outside the silica. Examples of ψ(r)-functions calculated for various Δ and N'_{seg} = 4 are shown in Figure S17a. It naturally extends to about $2R_{seg}+\Delta$, and its shape is the key to understanding the fish-shape profile in Figure S17b.

References

(1) Genix, A.-C.; Bocharova, V.; Carroll, B.; Lehmann, M.; Saito, T.; Krueger, S.; He, L.; Dieudonné-George, P.; Sokolov, A. P.; Oberdisse, J., Understanding the Static Interfacial Polymer Layer by Exploring the Dispersion States of Nanocomposites. *ACS Applied Materials & Interfaces* **2019,** *11* (19), 17863-17872.

(2) Cotton, J. P., Variations on Contrast in Sans: Determination of Self and Distinct Correlation Functions. *Adv. Colloid Interface Sci.* **1996,** *69*, 1-29.

(3) Mihut, A. M.; Dabkowska, A. P.; Crassous, J. J.; Schurtenberger, P.; Nylander, T., Tunable Adsorption of Soft Colloids on Model Biomembranes. *ACS Nano* **2013,** *7* (12), 10752-10763.

(4) Berndt, I.; Pedersen, J. S.; Richtering, W., Structure of Multiresponsive "Intelligent" Core-Shell Microgels. *J Am Chem Soc* **2005,** *127* (26), 9372-3.

(5) Stieger, M.; Richtering, W.; Pedersen, J. S.; Lindner, P., Small-Angle Neutron Scattering Study of Structural Changes in Temperature Sensitive Microgel Colloids. *The Journal of chemical physics* **2004,** *120* (13), 6197-6206.